# Hydrothermal waves in a disk of fluid

Nicolas Garnier, Arnaud Chiffaudel, and François Daviaud

Rayleigh-Bénard and Bénard-Marangoni instabilities have been studied for roughly a century and have served as prototypes for the transition to temporal chaos as well as spatiotemporal chaos of an initially stationary pattern. Using the Marangoni effect [1,2] with an horizontal temperature gradient to drive the system out of equilibrium, one can observe propagating waves instabilities: hydrothermal waves [3]. This paper presents different instability regimes of thermocapillary flows in extended geometry, focusing on propagating waves. We first introduce thermocapillary flows, and give some indications about physical effects involved. We then review experimental results in cylindrical geometry and illustrate how rich those systems are.

## 1 Thermocapillary flows

Thermocapillary effect arises when a temperature gradient is applied to a fluid with a free surface [2,4]. We consider here a disk of fluid with a free surface and an horizontal temperature gradient. The free surface is surrounded by ambient air.

### 1.1 Non-dimensional numbers

The fluid is characterized by its Prandtl number $Pr = \nu/\kappa$ which is the ratio of the diffusion coefficient of velocity to the one of temperature. But others numbers are important to describe the flow regime. We write $\rho$ the density and $\sigma$ the surface tension of the fluid. Those quantities depend on the temperature $T$, and one can define

$$\alpha = \frac{1}{\rho}\frac{\partial \rho}{\partial T} \qquad \text{as well as} \qquad \gamma = -\frac{\partial \sigma}{\partial T}\,.$$

$\alpha$ is always positive. $\gamma$ is also positive for pure fluids: when the temperature increases, interactions between molecules decrease, and so does the surface tension.

The existence of a free surface, and therefore surface tension, implies that one can compute a capillary length $\lambda_c$. This quantity represents the spatial extent on which surface energy is comparable to bulk energy —*e.g.* gravity—

*ie*, it represents the spatial extend on which surface tension effects are relevant for a layer of fluid at rest. In the presence of gravity, the capillary length reads:

$$\lambda_{\mathrm{c}} = \sqrt{\frac{\sigma}{\rho g}}\,,$$

where $g$ is the magnitude of the gravity field.

When the fluid depth $h$ is lower than $\lambda_{\mathrm{c}}$, surface tension is predominant over gravity, and conversely. In fact, the ratio of $h$ to $\lambda_{\mathrm{c}}$ is nothing less than the static Bond number $B\mathrm{o}$, also defined as the ratio of the surface tension forces to gravity:

$$B\mathrm{o} = \frac{\rho g h^2}{\sigma} = \left(\frac{h}{\lambda_{\mathrm{c}}}\right)^2 .$$

When the temperature is not uniform, buoyancy is present — represented by the Rayleigh number $R\mathrm{a}$ — as well as thermocapillarity — represented by the Marangoni number $M\mathrm{a}$. $R\mathrm{a}$ is constructed as the ratio of buoyancy forces to viscous forces and $M\mathrm{a}$ as the ratio of thermocapillary forces to viscous ones. If $\Delta T/l$ is the temperature gradient applied over distance $l$, they read:

$$R\mathrm{a} = \frac{\alpha g h^4}{\nu}\frac{\Delta T}{\kappa l} \qquad \text{and} \qquad M\mathrm{a} = \frac{\gamma h^2}{\rho\nu\kappa}\frac{\Delta T}{l}\,.$$

The dynamical Bond number $B\mathrm{d}$ is then defined as the ratio of thermocapillary forces to thermogravity forces:

$$B\mathrm{d} = \frac{R\mathrm{a}}{M\mathrm{a}} = \frac{\rho\alpha g h^2}{\gamma} = \left(\frac{h}{\lambda_{\mathrm{th}}}\right)^2 .$$

This defines another length scale $\lambda_{\mathrm{th}} = \lambda_{\mathrm{c}}\sqrt{\gamma/(\sigma\alpha)}$.

At ambient temperature (20°C), one has $\lambda_{\mathrm{c}} = 2.8$mm and $\lambda_{\mathrm{th}} = 88.5$mm for water. For the silicon oil we use, $\lambda_{\mathrm{c}} = 1.4$mm and $\lambda_{\mathrm{th}} = 3.0$mm.

This dimensional analysis suggests the existence of different flow regimes. It turns out that those regimes are observed in the experiments as giving rise to different pattern forming instabilities, as depicted in Fig. 1.

For higher fluid depth $h > \lambda_{\mathrm{th}}$, *i.e.* for thermogravity flows, one observes stationary patterns of rolls [5]; the axis of those rolls are parallel to the temperature gradient; those rolls have been observed in cylindrical geometry as well [6]. We are interested in wave patterns that appear in thermocapillary flows for $h < \lambda_{\mathrm{th}}$, among them are hydrothermal waves. Depending on the fluid depth, two types of hydrothermal waves are observed: type 1 (HW1) for medium fluid depth, and type 2 (HW2) for smaller fluid depth. Section 2 presents experimental observations of hydrothermal waves in the thermocapillary regime.

Finally, one also has to consider aspect ratios to discriminate if confinement is important or not. In the following, we assume large horizontal aspect

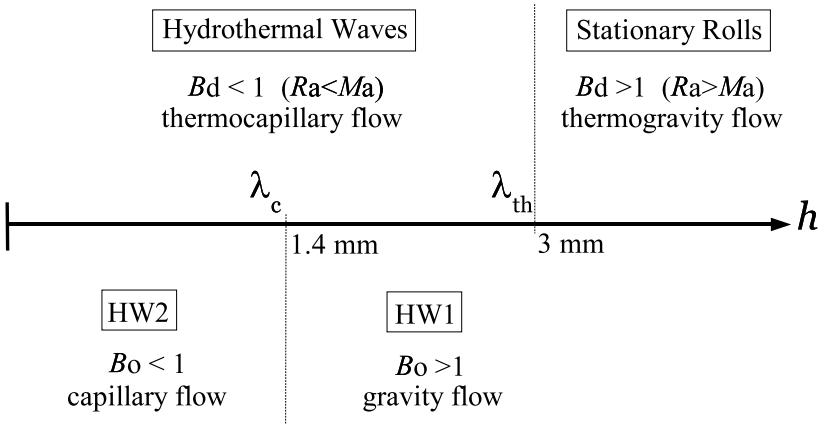


**Fig. 1.** Different regimes for thermocapillary and thermogravitational flow, depending on the fluid depth $h$. Limits are approximated by $h = \lambda_c$ and $h = \lambda_{th}$. We have precised instabilities into stationary rolls or hydrothermal waves which are observed experimentally in those different regimes. For hydrothermal waves, two types are observed (type 1, HW1, and type 2, HW2).

ratios, *i.e.* that the two horizontal directions (parallel and perpendicular to the temperature gradient) are much larger then the fluid depth $h$. In this case, confinement is negligible and we have an extended system in the two horizontal directions, as in the rectangular geometry of [7]. We are interested here in results obtained in cylindrical geometry. The curvature is then an additional parameter that can be defined locally; as we will discuss in § 2.3, one of its effects is to localize the wave-patterns [8].

### 1.2 Physical mechanisms

Let's now briefly give an heuristic description of instability mechanisms in a fluid layer submitted to a vertical or horizonal temperature gradient. Oblique temperature gradients have effects close to horizontal ones [9].

**Vertical temperature gradient: Bénard-Marangoni instability** Pearson [10] gave a simple mechanism to explain hexagons formation in Bénard-Marangoni convection. In that case, the temperature gradient is purely vertical and the fluid is at rest when the system is on the thermodynamic branch. If one considers a positive temperature perturbation at the surface of the fluid, then one deduces that due to a locally smaller surface tension at that point, the fluid is flowing away from that point. Due to mass conservation, this implies that fluid is flowing up to the point at the surface, from the bulk which is at a higher temperature. So the perturbation is amplified: there is instability.

**Horizontal temperature gradient** In that case a basic flow exists when the system is on the thermodynamic branch, and we expect an instability into propagating waves. Giving a physical mechanism for propagating waves is a more tedious exercise than it is for stationary patterns. In the case of thermocapillary flows, the time-oscillatory nature of the instability comes as a result of the existence of well-defined profiles for the temperature and the velocity in the basic flow. A relevant mechanism has to involve features from those profiles such as the local sign of the horizontal and vertical temperature and velocity gradients. Smith [11] expressed two different mechanisms depending on the Prandtl number. Each of those is based on the Pearson mechanism, but whereas this former is $Pr$ independent, Smith considered the extreme cases of a flow dominated by inertial effects ($Pr \to 0$) or by viscous effects ($Pr \to \infty$). The relaxation of temperature and velocity perturbations are then occurring on very different time scales. Depending on the signs of the underlying temperature and velocity gradients, an oscillatory behavior is shown to be unstable and to propagate along the horizontal temperature gradient (small $Pr$), or perpendicularly to it (large $Pr$).

It is worth mentioning that hydrothermal waves are an instability mode present in the absence of surface deflections, *i.e.*, assuming that the free surface is non-deformable. Taking into account surface deflections as in [12] may lead to another instability mode. Our experiments suggest that fluid depth variations are small compared to the fluid depth so that they can be neglected. The stability analysis of [3,13] is then valid.

## 2 Experiments

We now present some experimental results, focusing on extended cylindrical geometries, with large horizontal aspects ratios. A sketch of the experimental cell is reproduced in Fig. 2. The setup allows us to work at various fluid depths $h$ while always having no meniscus on the side walls [14] and thus a perfectly homogeneous fluid depth $h$. We define the control parameter as $\Delta T = T_{\text{ext}} - T_{\text{int}}$. This quantity can be positive or negative, and both cases are not equivalent, due to the presence of curvature [8].

We use silicon oil of Prandtl number 10 and work with $h < \lambda_{\text{th}} = 3\text{mm}$ to have hydrothermal waves. Both cases $h \gtrless \lambda_{\text{c}} = 1.4\text{mm}$ are studied. Figure 3 gives a phase diagram of the experiment. Detailed observations and precise measurements have been performed for $h = 1.2\text{mm}$ (small $Bo$) and $h = 1.9\text{mm}$ (large $Bo$) for both positive and negative $\Delta T$ and are reproduced on Fig. 3, left. The inset of Fig. 3 (right) shows accurate determinations of HW1 and HW2 instability onsets for $\Delta T > 0$. The onset of each mode is determined by searching at which value of $\Delta T$ the squared amplitude of the corresponding pattern is vanishing, following a linear law. By doing so, we also check that each instability is supercritical.

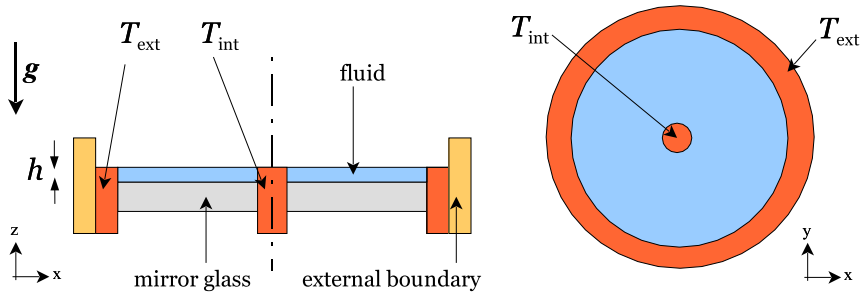


**Fig. 2.** Sketch of the experimental cell. External diameter is 135mm, fluid depth $h$ is of order 1 mm and $\Delta T = T_{\rm ext} - T_{\rm int}$ is of order 10K.

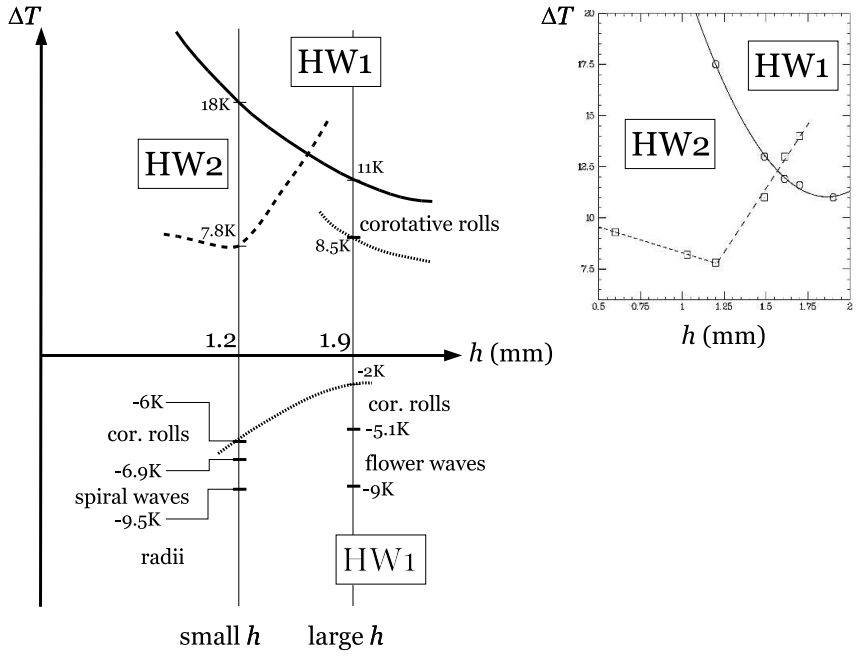


**Fig. 3.** Experimental phase diagram in a cylindrical cell. Left: general view. Right: precise measurements of HW1 (○) and HW2 (□) onsets.

We report in table 1 the experimental values of the critical temperature difference for the wave instabilities. The critical values of the Rayleigh $R$a and Marangoni $M$a numbers are also reported.

| fluid depth | $\Delta T_c$ | $R\mathrm{a}_c$ | $M\mathrm{a}_c$ | pattern |
|---|---|---|---|---|
| $h = 1,2$ mm | 7,8 K | 80 | 500 | HW2 |
| | 18 K | 190 | 1150 | HW1 |
| $h = 1,9$ mm | 11 K | 735 | 1760 | HW1 |
| | $-5,2$ K | 350 | 830 | flowers |
| | $-10$ K | 670 | 1600 | HW1 |

**Table 1.** Critical values at the onset of time-oscillatory patterns.

As can be seen on the phase diagram, the system exhibits a large variety of pattern-forming instabilities. This richness cannot be inferred from the dimensional analysis of the previous section. The next paragraph details each of the observed structures.

### 2.1 $T_{\mathrm{int}} < T_{\mathrm{ext}}$

**Large Bond number (large fluid depth)** For higher Bond numbers, the basic thermocapillary flow composed of a single large roll is stable as long as $\Delta T < 8.5$K. For $\Delta T > +8.5$K a structuring of the basic flow occurs: concentric corotative rolls exist. These rolls first appear close to the hot side of the container, then invade all the cell, as represented on Fig. 4. For higher temperature gradient ($\Delta T > +11$K), hydrothermal waves appear. The corresponding pattern is composed of spiraling waves. Two realizations are presented in Fig. 5. A source of waves with a large spatial extension may be present, as well as a (smaller) sink, and those objects separate two regions of right- and left-turning waves. On some realizations, a single wave (right- or left-turning) is present. In both cases, the two components of the local wavenumber are proportional, and their ratio is roughly constant anywhere in the cell and does not depend on the control parameter. Those hydrothermal waves are called HW1. They are also observed in rectangular geometries [5,7,15] and are well described by linear stability analysis [3,13].

HW1 propagate with an angle from the temperature gradient. The radial propagation, *i.e.* the propagation along the temperature gradient, is always from the cold center ($T_{\mathrm{int}}$) towards the hot perimeter ($T_{\mathrm{ext}} = T_{\mathrm{int}} + \Delta T$). The orthoradial propagation is either to the right or to the left, both cases having equal probability.

**Small Bond number (small fluid depth)** For lower Bond numbers, and increasing the temperature difference $\Delta T$ from 0K, no structuring of the basic flow by stationary corotative rolls is observed. The first instability mode

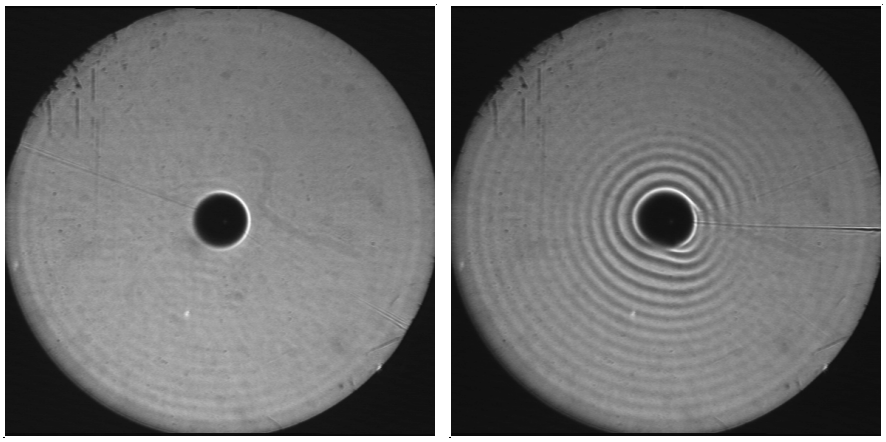

**Fig. 4.** Shadowgraph images for $h = 1.9$mm and cold center. Stationary corotative rolls appear on the hot side of the container (left: $\Delta T = +10$K), and invade all the radial extension for higher temperature gradient (right: $\Delta T = +11.75$K).

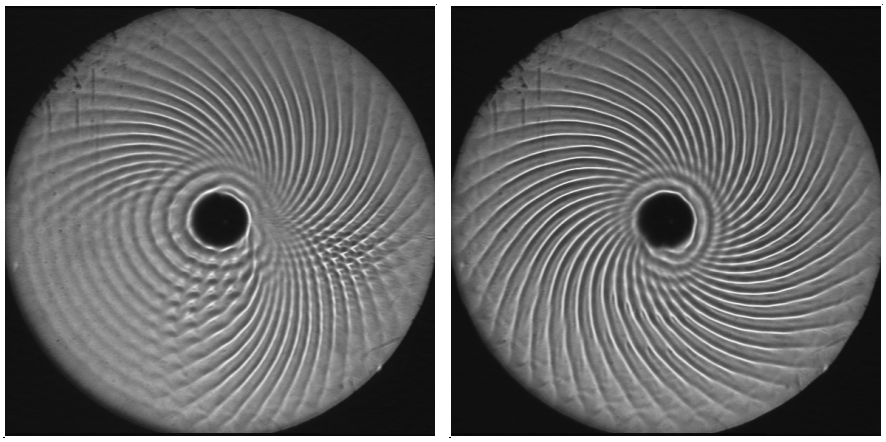

**Fig. 5.** Shadowgraph images for $h = 1.9$mm and cold center. left: $\Delta T = +13$K, right: $\Delta T = +14.25$K. Hydrothermal waves of type I (HW1) in the shape of rotating spirals are appearing on top of the stationary rolls pattern. On the left, the pattern is composed of a uniform right-turning spiral.

appears for $\Delta T > 7.8$K; it is a bidimensional hydrothermal wave (HW2) [14] localized near the center of the cell. At onset, the wavevector of the pattern is purely radial and the propagation is from the cold center towards the hot perimeter. As the control parameter is increased, the orthoradial component is growing from zero. So the spatial structure of the HW2 mode evolves from a pulsing target to a spiraling pattern. Increasing the temperature gradient

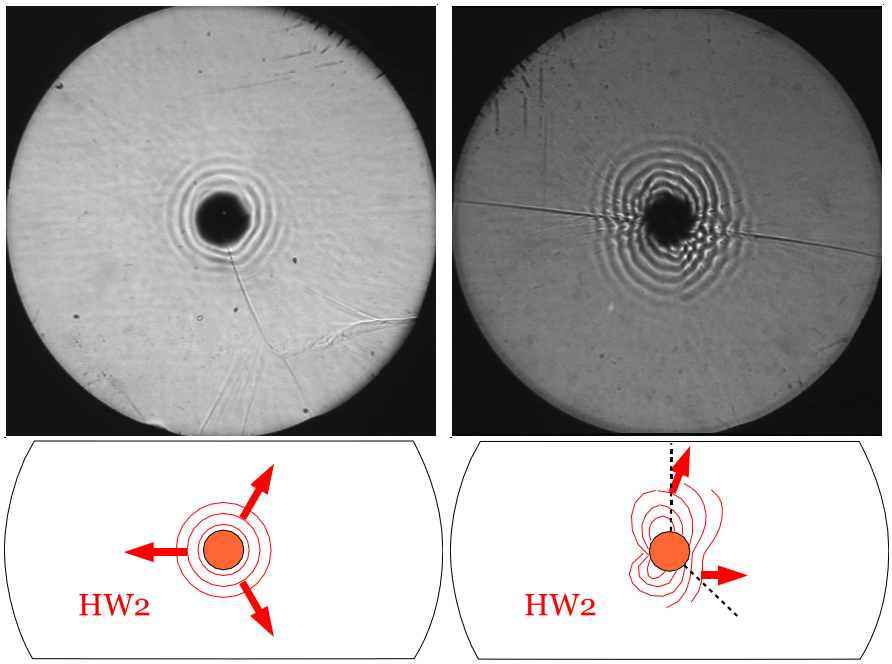


**Fig. 6.** $h = 1.2$mm and cold center. Hydrothermal waves of type II (HW2). Close to onset (left: $\Delta T = +8.5$K), the pattern is composed of pulsing targets and the wavevector is purely radial. Further in the supercritical region (right: $\Delta T = +12$K), the wavevector has an additional azimuthal component. No stationary pattern is present. Arrows on the schematics represent the phase velocity.

also results in an extension of the domain occupied by the HW2 pattern (Fig. 6).

For larger temperature gradients, HW1 appear in the whole domain of the cell where HW2 have a small or vanishing amplitude (Fig. 7). Measurements of the local frequency and of the local wavenumber along the radial direction allow one to distinguish HW1 and HW2 instability modes. We have measured the onset of HW1 on top of the HW2 pattern, and shown that the two modes do not interact close to the onset of the second one (HW1). For higher temperature gradient, interactions occur and the overall pattern is spatio-temporally chaotic.

### 2.2 $T_{\mathrm{int}} > T_{\mathrm{ext}}$

When the center is heated with respect to the outside perimeter, the dynamics is less coherent and more localized near the hot center; the phase diagram in the region $\Delta T < 0$ is richer.

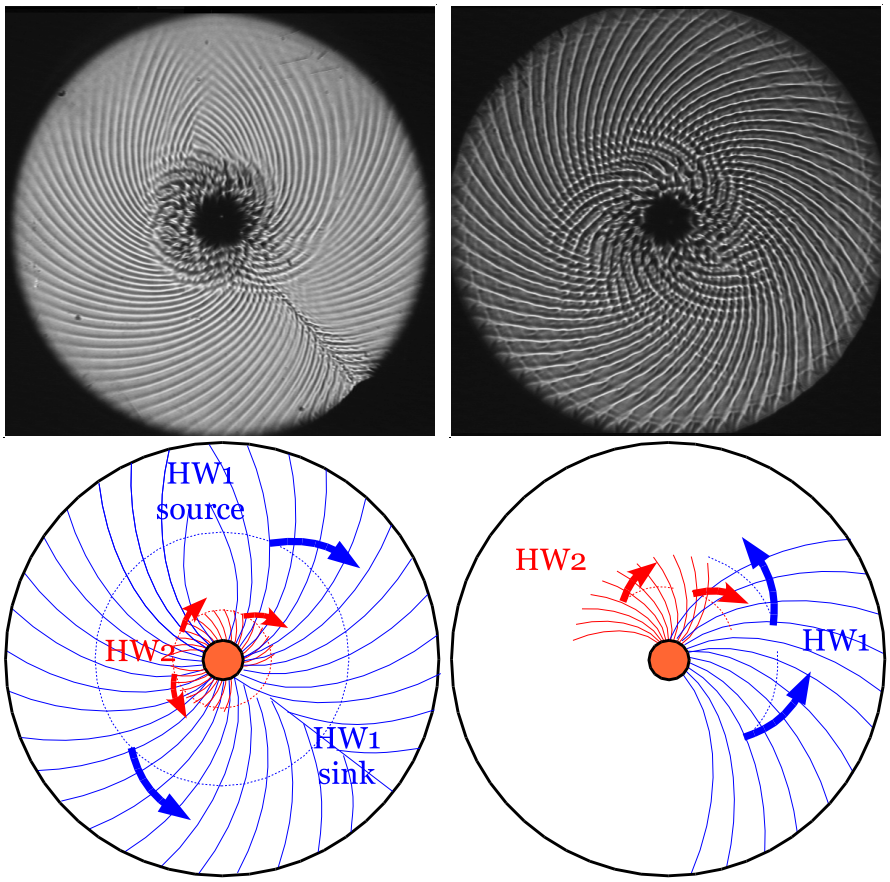


**Fig. 7.** $h = 1.2$mm and cold center, $\Delta T = +20$K. HW2 are localized near the center. The HW1 pattern is either composed of right- and left-propagating waves (left photograph) or of a single wave (right photograph). Both configurations are unstable and the system oscillates randomly between the two regimes. The schematics detail propagation directions and source/sink positions for each realization. The radial propagation is always from the center and towards the perimeter.

**Large Bond number (large fluid depth)** For $-2\text{K} < \Delta T < 0\text{K}$, the basic flow is stable. The first instability is stationary, and as in the case $\Delta T > 0$, it consist of a structuring of the base flow by corotative rolls. Those rolls appear on the hot side of the container, *i.e.* around the inner cylinder for $|\Delta T| > 2\text{K}$ (Fig. 8, left).

For $|\Delta T| > 5.1K$, a time-oscillatory instability develops around the hot center. At onset, we observe a rotating hexagon (Fig. 8, right). When the temperature gradient is increased, each corner of the hexagon moves away from the center, and the pattern takes the shape of a flower (Fig. 9). While

increasing $|\Delta T|$, one observes an elongation of the petals, then the apparition of a seventh petal (due to a modulational instability like the Eckhaus instability in the azimuthal direction). Outside the flower, a structure is present with the same azimuthal wavenumber and it evolves with $|\Delta T|$ to form visible branches that rotate at the same angular frequency as the flower.

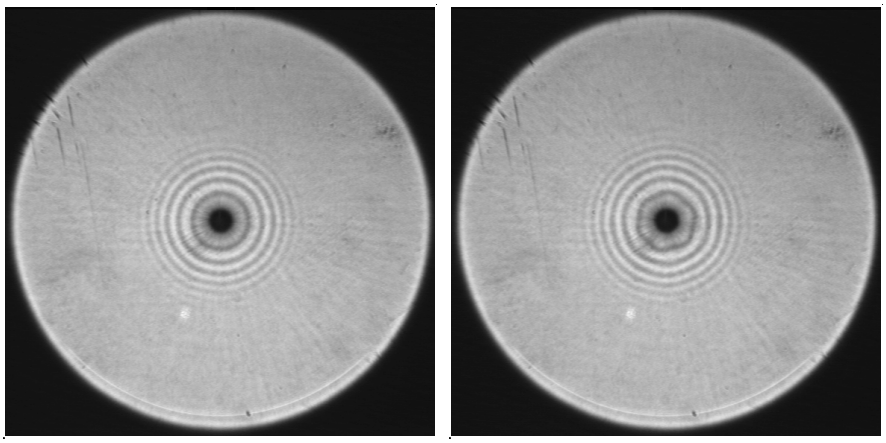

**Fig. 8.** $h = 1.9$mm and hot center. left: $\Delta T = -5$K, Stationary corotative rolls are present close to the hot center of the cell. right: $\Delta T = -5.2$K, same stationary rolls, with an additional hexagon turning around the center.

For $\Delta T < -9$K, HW1 appear. Again, their radial propagation is from the cold side towards the hot side; so the HW1 pattern is such that energy flows from the external perimeter to the center. As we will detail further, this situation is not confortable and the structure has a strong tendency to be incoherent. Fig. 10 presents a spatio-temporally chaotic realisation for a large value of the control parameter. Stationary rolls are visible, and HW1 are barely recognizable.

**Small Bond number (small fluid depth)** First, for small $|\Delta T|$, only the basic flow is observed. For $\Delta T < -6$K, corotative rolls appear near the center. Their wavelength is small because it scales with the fluid depth which is small in that case. The amplitude of this stationary pattern is small and the corresponding shadowgraphic signal is very weak. Then, for $\Delta T < -6.9$K, spiral waves appear on top of the corotative rolls. We believe those are hydrothermal waves. Like HW2, they are localized near the center and their radial and azimuthal wavenumbers are not constant in space. An example is reproduced in Fig. 11, left. The radial component of the wavevector is pointing toward the center, and the pattern is a left-turning wave. So the

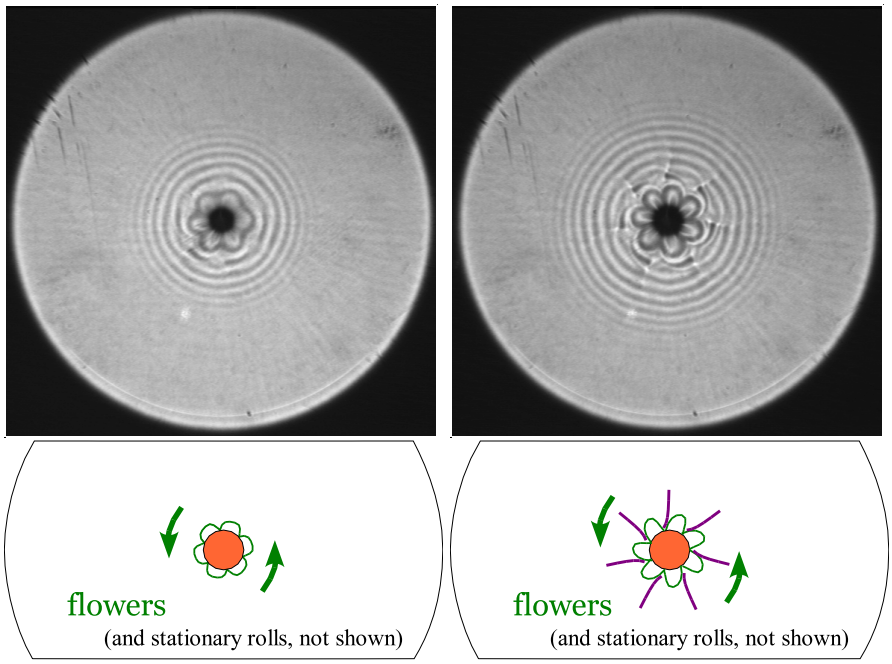


**Fig. 9.** $h = 1.9$mm and hot center. left: $\Delta T = -5.6$K, a six-petals flower is turning. right: $\Delta T = -7$K, an additional wavelength has appeared, as well as branches in between the petals, outside the flower.

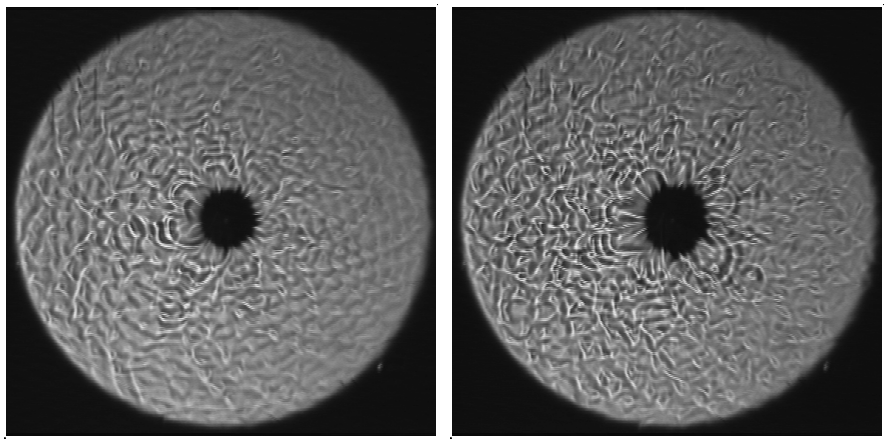

**Fig. 10.** $h = 1.9$mm and hot center; left: $\Delta T = -15.0$K, right: $\Delta T = -20.0$K. Hydrothermal waves of type 1 have appeared on top of the flower pattern. Because the radial component of the HW1 wavevector is pointing toward the center of the cell, the spatial coherence of the resulting structure is small, and the overall pattern is spatio-temporally chaotic.

radial direction of propagation is reversed compared to an HW1 (or HW2) pattern of the same chirality obtained for $\Delta T > 0$.

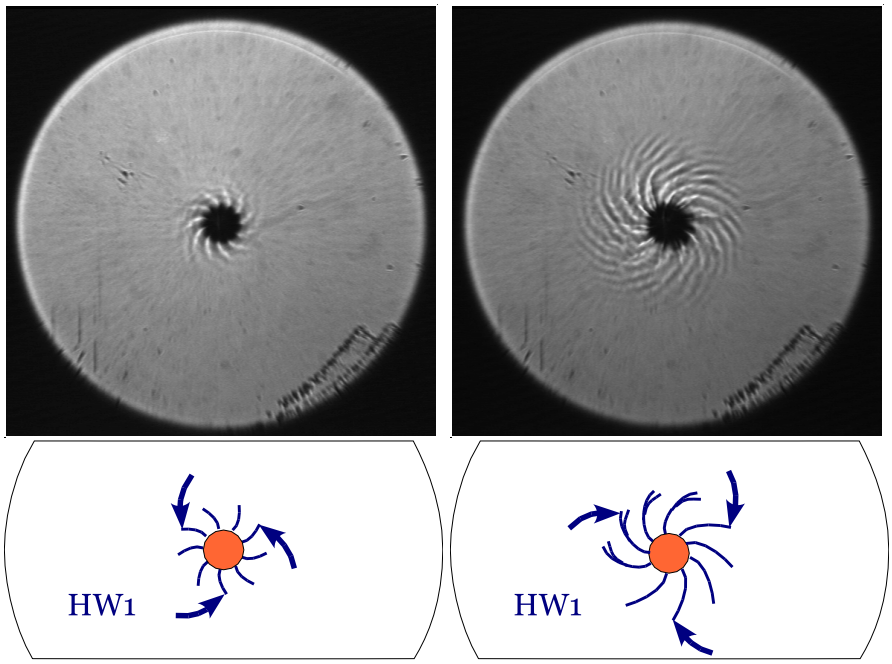


**Fig. 11.** $h = 1.2$mm and hot center. left: $\Delta T = -8$K, left-turning spiral waves. right: $\Delta T = -11$K, right-turning spiral waves and radii. Radial propagation of the spirals is from the external perimeter towards the inner plot. (Radii are not shown on the schematics).

For $\Delta T < -9.5$K, another propagating structure appear around the center of the cell. This structure has a wavevector which is purely azimuthal, so we label it "radii" as well. They are visible on Fig. 11, right, very close to the inner cylinder. We observed that radii have a frequency close to twice the one of hydrothermal waves. The azimuthal wavenumber is the same so the azimuthal phase velocity of the radii is twice the one of the spirals. This allows us to conclude that they are different instabilities, though they may be 1:2 resonant. The strong localization of the radii suggests that it may be an instability of the hot boundary layer.

### 2.3 Curvature and localization

We can interpret to some extent the above observations using local curvature as introduced in [8]. The first effect of curvature is to distribute the temperature with an hyperbolic profile in the radial direction. This implies that

the temperature gradient is larger in magnitude close to the center. For this reason, it is clear that the region close to the center becomes supercritical before the rest of the cell. This explains why most of the wave-patterns we observe appear first close to the center, and afterwards in the bulk.

A second effect of curvature is to constraint the wavevectors. Close to the center, the azimuthal direction is not as extended as it is further from the center. This implies that to keep a constant value of the wavenumber, the pattern has to increase the number of wavelengths in the azimuthal direction, and reduce the wavelength in the radial direction.

Moreover, in the case of hydrothermal waves, and in particular of HW1, the radial propagation is always from the cold to the hot side. In one-dimensional geometries [17–19], it has been checked that phase and group velocities point towards the same direction; this property seems satisfied as well in 2D. When the center is colder than the outside, the pattern propagates from the center, and therefore spreads in the azimuthal direction. This can be achieve while keeping the spatial coherence. In the opposite case when the outside perimeter is colder than the center, the propagation is from the outside towards the inside, and the information (or energy) of the structure has to converge from an extended region to a confined one; in that case, any inhomogeneity of the structure (wavenumber, frequency or amplitude) in the azimuthal direction will result in a destruction of the coherence of the converging process. For example, if the amplitude of the pattern is locally smaller at some given angle in the cell, the equivalent of a Bénard cell at that point will be squizzed by neighboring cells of larger amplitude, which will result in a decrease of the wavelength, and therefore of the amplitude: there is instability. This will ultimately result in the disappearance of the cell (*i.e.*, of one wavelength), and the nucleation of modulations of, e.g., the amplitude. Those modulations will be amplified by the same mechanism while the pattern converges towards the center. All those events occur incoherently in time and in space, giving rize to a turbulent pattern more easily when $T_{\mathrm{int}} > T_{\mathrm{ext}}$ than in the reverse case.

### 2.4 About rectangular geometries

We have also conducted experiments in rectangular geometry. In that case, positive and negative temperature gradients are equivalent, and one recovers the same behaviors: HW1 for high $Bo$ and HW2 for low $Bo$. As in previous experiments [5,15,16], we found that corotative rolls appear only for large $Bo$, and prior to the HW1 instability; the HW1 are emitted by "line"-sources which extend over the whole extension between the hot and the cold sides. For smaller depth $h < \lambda_{\mathrm{c}}$, HW2 are observed; they are emitted by ponctual sources located on the cold side of the container [5]. Moreover, for large fluid depth and therefore large Bond number, hydrothermal waves instability is replaced by the stationary instability into parallel rolls with axis aligned with the temperature gradient, as presented in Fig. 1.

## 3 Applications

Many quantitative results have been obtained for hydrothermal waves, on the theoretical side (linear stability analysis [3,8,9,13]) as well as on the experimental side [4,5,7,14–16]. For more fundamental studies, hydrothermal waves represent an ideal experimental nonlinear waves system. As Bénard cells, hydrothermal waves are not just nice-looking; we have used them to study the transition to spatio-temporal chaos of a traveling waves system. In one horizontal dimension, they are well modeled by a complex Ginzburg-Landau equation [17,18]. As their group velocity is finite, they are subject to the convective/absolute distinction [17,19], not only for their primary onset, but also for the onset of their secondary instabilities.

One century after the pioneering work of Henri Bénard, thermocapillary flows are still a promising field of research not only on the hydrodynamical point of view — including challenging fundamental and applied industrial studies [1] — but also as a robust model for the study of nonlinear waves and spatiotemporal chaos.

*Acknowledgments* This work has been done in the *Groupe Instabilités et Turbulence*, SPEC, CEA Saclay. At the time of writing, N. G. was supported by a Joseph Ford fellowship from the *Center for Nonlinear Sciences*, Georgia Institute of Technology. Discussions with J. Burguete and G.P. Neitzel are acknowledged.

## References

1. D. Kuhlman: *Thermocapillary Flows*, (Springer, New York 1999)
2. S.H. Davis: Ann. Rev. Fluid Mech. **19**, 403 (1987)
3. M.K. Smith, S.H. Davis: J. Fluid Mech. **132**, 119 (1983)
4. M.F. Schatz, G.P. Neitzel: Annu. Rev. Fluid Mech. **33**, 93 (2001)
5. J. Burguete *et al*: Phys. Fluids **13**, 2773 (2001)
6. E. Favre *et al*: Phys. Fluids **9**, 1473 (1997)
7. M.A. Pelacho *et al*: Phys. Rev. E **62**, 477 (2000)
8. N. Garnier, C. Normand: C. R. Acad. Sci., Ser. IV **2** (8) 1227 (2001)
9. A.A. Nepomnyashchy *et al*: J. Fluid Mech. **442**, 141 (2001)
10. J.R. Pearson: J. Fluid Mech. **19**, 489 (1958)
11. M.K. Smith: Phys. Fluids **29**, 3182 (1988)
12. M.K. Smith, S.H. Davis: J. Fluid Mech. **132**, 145 (1983)
13. J-F. Mercier, C. Normand: Phys. Fluids **8**, 1433 (1996)
14. N. Garnier, A. Chiffaudel: Eur. J. B **19**, 87 (2001)
15. R.J. Riley, G.P. Neitzel: J. Fluid Mech. **359**, 143 (1998)
16. M.A. Pelacho, J. Burguete: Phys. Rev. E **59**, 835 (1999)
17. N. Garnier: Ondes non-linéaires à une et deux dimensions dans une mince couche de fluide. Ph.D. Thesis, University Denis Diderot, Paris 7 (2000)
18. N. Garnier *et al*: Physica D **174**, 1 (2003)
19. N. Garnier *et al*: Physica D **174**, 30 (2003)